ELSEVIER

Surface Science 384 (1997) 315–333

surface science

Mechanism of the partial oxidation of ethylene on an Ag surface: dipped adcluster model study

Hiroshi Nakatsuji [a,b,c,*], Hiromi Nakai [d], Keiji Ikeda [a], Yoko Yamamoto [a]

[a] *Department of Synthetic Chemistry and Biological Chemistry, Graduate School of Engineering, Kyoto University, Sakyo-ku, Kyoto 606-01, Japan*

[b] *Department of Applied Chemistry, Graduate School of Engineering, The University of Tokyo, Hongo, Tokyo 113, Japan*

[c] *Institute for Fundamental Chemistry, 34-4, Takano-Nishihiraki-cho, Sakyo-ku, Kyoto 606, Japan*

[d] *Department of Chemistry, School of Science and Engineering, Waseda University, Shinjuku-ku, Tokyo 169, Japan*

Received 11 September 1996; accepted for publication 1 April 1997

Abstract

The partial oxidation of ethylene to ethylene oxide catalyzed by silver is studied by the ab-initio Hartree–Fock and MP2 methods using the dipped adcluster model (DAM). The active species is the superoxide O_2^- which is molecularly adsorbed in a bent end-on geometry on the silver surface. Ethylene reacts with the terminal oxygen atom and the reaction proceeds smoothly without a large barrier to yield ethylene oxide. The complete oxidation of ethylene involving the superoxide is forbidden due to the existence of a large energy barrier. This is one origin of high selectivity. Without the silver surface, the epoxidation reaction is very unfavorable, showing the catalytic activity of the silver surface. The atomically adsorbed oxygen seems not to be selective: it gives both ethylene oxide and complete oxidation products. Therefore, adding to the selectivity due to the superoxide, an overall selectivity larger than 6/7 can be possible. In the process yielding ethylene oxide from atomic oxygen, electron transfer and back-transfer from/to the metal are important processes which can be promoted by both electron donor and acceptor. Detailed electronic mechanisms are clarified and discussed. © 1997 Elsevier Science B.V.

Keywords: Ab initio Hartree–Fock (HF) and second-order Møller–Plesset (MP2) methods; Atomic oxygen; Catalytic activity of silver; Combustion; Dipped adcluster model (DAM); Epoxidation; Ethylene oxide; Reaction mechanism; Superoxide

1. Introduction

The partial oxidation of ethylene to ethylene oxide is a very important catalytic reaction in the chemical industry. The only effective catalyst for this reaction is silver [1–3]. While numerous reports [4–21] have been published, the origin of this unique catalytic activity of silver has not yet been clarified.

Experimental studies [22–36] using surface spectroscopic techniques have revealed the existence of at least four oxygen species adsorbed on a Ag surface: physisorbed species (O_2), molecularly adsorbed species, superoxide (O_2^-) and peroxide (O_2^{2-}), and atomically adsorbed species (O^- and/or O^{2-}). On the other hand, ethylene is not adsorbed on a clean silver surface [1–3,5,6]. These results support the reaction mechanism proposed by Twigg, i.e. ethylene in the gas phase reacts with the adsorbed oxygen on the silver surface [4].

Among the various adsorbed oxygen species,

* Corresponding author. Fax: +81 75 7535910.

PII S0039-6028(97)00239-2

the active species for the partial oxidation of ethylene has not yet been identified. Many studies support the notion that molecularly adsorbed oxygen is the active species for partial oxidation, while total oxidation involves atomically adsorbed oxygen [8,11]. Herzog showed that atomically adsorbed oxygen produced from N_2O gave only CO_2 and H_2O at low temperature, at which surface migration cannot occur [8–10,12]. Campbell compared the reactivity of Ag(111) with Ag(110). The coverage of atomically adsorbed oxygen on the Ag(111) surface is lower than that on Ag(110). The selectivity of ethylene oxide formation is higher on Ag(111) [13]. However, recent experimental results giving a selectivity of higher than 6/7 may conflict with the mechanism which assumes only molecularly adsorbed oxygen as the active species.

If only molecularly adsorbed oxygen is involved in the partial oxidation and the atomically adsorbed species gives CO_2 and H_2O by complete oxidation, the overall reaction on the silver surface can be written as

$$O_2(g) \rightarrow O_2(a), \quad (1)$$

$$C_2H_4(g) + O_2(a) \rightarrow C_2H_4O(g) + O(a), \quad (2)$$

and

$$C_2H_4(g) + 6O(a) \rightarrow 2CO_2(g) + 2H_2O(g). \quad (3)$$

The following equation is obtained from Eqs. (1)–(3):

$$7C_2H_4(g) + 6O_2(g) \rightarrow 6C_2H_4O(g) + 2CO_2(g) + 2H_2O(g). \quad (4)$$

Eq. (4) shows that ethylene oxide is formed from ethylene at a maximum selectivity of 6/7 (85.7%) [37]. However, some recent experiments have exceeded this limit, and have achieved a selectivity of 85–87% by adding NaCl to the catalyst [14,15]. Based on these results, it has been suggested that the reaction may proceed by a mechanism which differs from that described above. Van Santen and de Groot have showed the reactivity of atomically adsorbed oxygen: both ethylene oxide and carbon dioxide were obtained in the absence of molecularly adsorbed oxygen [18]. Deng et al. studied the promoting effects of Re and Cs, and concluded that Re and Cs could enhance the selectivity, reaching a value of over 85.7% [19–21].

Previous theoretical studies have suggested that the active species for epoxidation is atomic oxygen. Carter and Goddard studied this reaction in detail using the ab-initio generalized valence bond correlation consistent configuration interaction (GVB-CCCI) method [38,39]. They concluded that the surface atomic oxyradical anion (SAO) is selective for the formation of ethylene oxide, and proposed that the key to high epoxidation yields is to keep the oxygen coverage above $\theta = 0.5$ to ensure a large concentration of SAO. Van den Hoek et al. investigated the role of subsurface oxygen [40]. They showed that ethylene reacts with adsorbed atomic oxygen to form epoxide, and that subsurface oxygen enhances epoxide formation by chemisorbed oxygen. Jørgensen and Hoffmann studied this reaction using extended Hückel calculations [41]. These papers concluded that atomically adsorbed oxygen is active for partial oxidation.

In our previous papers [42–44], we studied theoretically the electronic structures and geometries of molecularly and dissociatively adsorbed oxygens on the Ag surface and the inter-conversions between them. In this paper, we calculate the energy diagrams of the reaction of ethylene with molecularly adsorbed oxygen and atomically adsorbed oxygen. The calculations are performed using the ab-initio Hartree–Fock (HF) and second-order Møller–Plesset (MP2) methods. The dipped adcluster model (DAM) [45,46] is used to include the effects of the bulk metal, such as electron transfer between the admolecule and the surface and the image force. The DAM has been successfully applied to the oxygen chemisorption on a silver surface [42–44], and to harpooning, surface chemiluminescence and electron emission in the halogen/alkali-metal surface system [47]. A review on the DAM study has been published recently [46].

The present calculations indicate that the molecularly adsorbed oxygen is the primary active species in partial oxidation, and that atomically adsorbed oxygen contributes less selectivity to both partial and complete oxidation. We clarify the mechanisms of the reactions and the role of the silver surface.

2. Computational details

Ethylene is not adsorbed on a clean Ag surface, so we assume that both epoxidation and total oxidation of ethylene proceed in the Eley–Rideal mode, which corresponds to the reaction between the adsorbed oxygen species and gaseous ethylene. In the present study, the reactions of ethylene with molecular and atomic oxygen species are examined using the DAM combined with the ab-initio MO method. Previously, we studied the O_2/Ag system [42–44], and showed that molecularly adsorbed oxygen exists in two stable geometries, i.e. the end-on (bent) on-top structure and the side-on bridge structure. The former geometry is expected to be electronically more favorable for reactions with ethylene.

In the present study, the electron exchange between the admolecule and the surface is taken into account by the DAM. The potential energies of the adcluster with and without electron transfer from the bulk metal, namely $n=1$ and 0, are calculated by the ab-initio HF method. The restricted HF (RHF) method is used for closed-shell systems, and the unrestricted HF (UHF) method for open-shell systems. The geometries of the reactants, products and intermediates are optimized at the HF level. The geometries of the transition states (TSs) are calculated using the force constant matrix at the HF level; namely, the energy gradient is zero and the force constant matrix has only one negative eigenvalue at the TS. The electrostatic interaction energy between the adcluster and the bulk metal is estimated by image force correction [45,46]. The electron correlations are included by the MP2 method. The calculations were performed using the GAUSSIAN92 software package [48].

The Gaussian basis set for the silver atom is the (3s3p4d)/[3s2p2d] set, and the Kr core is replaced by the relativistic effective core potential [49]. For oxygen, we use the (9s5p)/[4s2p] set of Huzinaga and Dunning [50,51] augmented by the diffuse s and p functions of $\alpha=0.059$ as anion bases [52]. Polarization d functions of $\alpha=2.704$ and 0.535 [53] are added to the oxygen basis set in the MP2 calculations. Generally speaking, the effect of the polarization function is larger in the post-HF calculation than in the HF calculation. For carbon and hydrogen, the (9s5p)/[4s2p] and (4s)/[2s] sets of Huzinaga and Dunning are adopted, respectively [50,51].

In Appendix A, the accuracy of the present method is investigated for the basis set and the electron correlation effect.

3. Reactions with molecularly adsorbed oxygen

3.1. Epoxide formation

Here, we study the epoxidation reaction of ethylene with the molecularly adsorbed superoxide on a silver surface. We first examined the favorable pathway of ethylene attack onto the superoxide on the Ag surface. The most favorable pathway is illustrated in Fig. 1: the C–C bond of ethylene lies in the same plane as Ag_2O_2, keeping the molecular plane of ethylene perpendicular to this plane, and

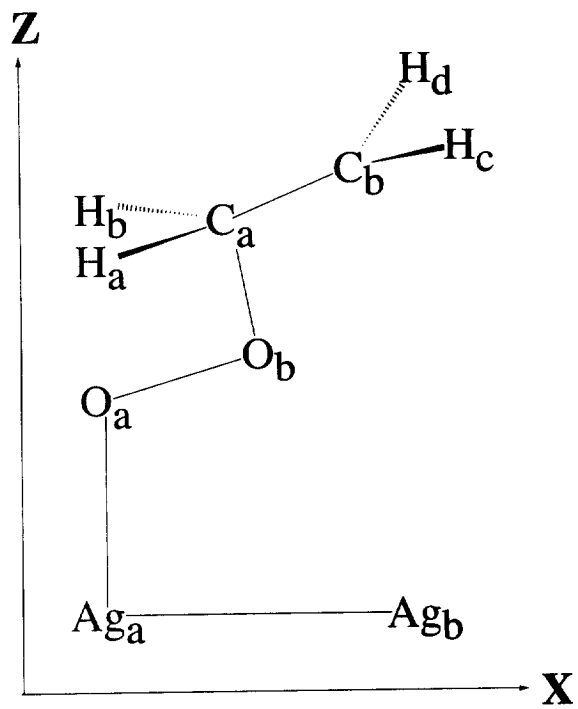

Fig. 1. Model adcluster used in this study. Geometries are optimized in the C_s symmetry except for the Ag–Ag distance and the O_a–Ag–Ag angle, fixed at 2.8894 Å and 90°, respectively.

approaches the terminal oxygen atom unsymmetrically. We have examined other possible approaches of ethylene, and the result is summarized in Appendix B. After examining this favorable geometry, we kept the $Ag_2O_2C_2H_4$ adcluster in the C_s symmetry throughout the reaction. The adcluster is placed on the x–z plane, and the Ag–Ag bond is parallel to the x axis. The same atoms are denoted by subscripts (such as O_a and O_b) for convenience. The intermediates and the TSs along the reaction pathway are optimized at the HF level with the Ag–Ag distance and the Ag_b–Ag_a–O_a angle fixed at 2.8894 Å and 90.0°, respectively. Other geometrical parameters are fully optimized along the reaction path.

Fig. 3 shows the energy diagram for the epoxidation reaction between gaseous ethylene and molecular superoxide species on the Ag_2 cluster handled by the DAM. The potential energy of the reacting system is calculated by the MP2 method including the image force correction. In Fig. 2, the reaction proceeds from left to right, and the energy scale on the left is in kcal mol^{-1} relative to the free system (i.e. $Ag_2+O_2+C_2H_4$). The optimized structures of the intermediates and the TSs are also illustrated in Fig. 2.

The energy diagram given in Fig. 2 shows that this reaction proceeds very smoothly: the reaction is exothermic, there are no very high barriers, and there are no overly stable intermediates. We therefore conclude that epoxide formation from the superoxide species on a silver surface proceeds very smoothly.

We note that the exothermicity of the overall reaction is partially due to the formation of the atomically adsorbed oxygen on the silver surface. This will become clear later, when we take off the silver surface and calculate the reaction between ethylene and gaseous oxygen.

We examine each reaction step shown in Fig. 2. The first step of this reaction is the molecular adsorption of O_2 on the Ag surface, in which one electron is transferred from the bulk metal to the adcluster (i.e. $n=1$). The transferred electron mainly occupies the out-of-plane π^* orbital of O_2, and the in-plane π^* MO of O_2 remains singly occupied. The optimized geometry is bent end-on, as shown previously [42–44]. The ground state for the end-on adsorption of O_2 is the superoxide. Although there is another superoxide species, in which the in-plane π^* MO of O_2 is doubly occupied and the out-of-plane π^* MO is singly occupied, at a slightly higher energy level, this species is not favorable for reaction with ethylene in this reaction

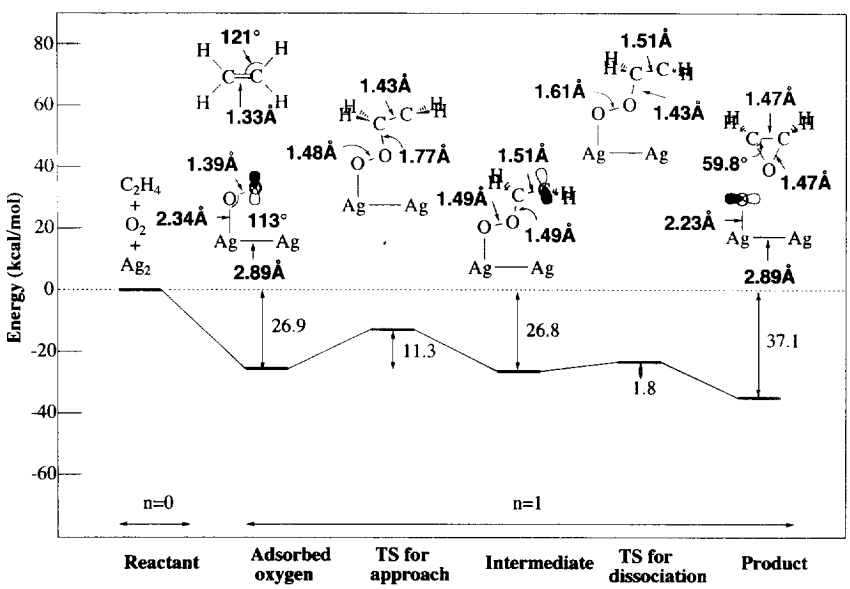

Fig. 2. Energy diagram for the reaction between ethylene and molecularly adsorbed oxygen, calculated by the MP2 method.

pathway. The adsorption energy of the superoxide is calculated to be 7.4 kcal mol^{-1} at the UHF level and 26.9 kcal mol^{-1} at the MP2 level. The experimental molecular adsorption energies are 9.2, 9.3, and 24.1 kcal mol^{-1} for the Ag(111) [34], Ag(110) [34] and electrolytic Ag [54] surfaces, respectively.

The next step is the attack of ethylene onto the terminal oxygen atom O_b: the reaction site of the molecularly adsorbed superoxide [42–44]. It leads to the TS and the intermediate with an energy barrier of 11.3 kcal mol^{-1}. The energy level of the intermediate is similar to that of the initial step. The process leading to the TS includes the formation of an s-bond between O_b and C_a and the breaking of the in-plane π bond of O_2 and the π bond of C_2. The O_a–O_b distances of the adsorbed oxygen state, the TS, and the intermediate are 1.39, 1.48, and 1.49 Å, respectively, which is compared with 1.47 Å for the peroxide on Ag(110) [28,29]. The O_b–C_a distances of the latter two are calculated to be 1.77 and 1.49 Å, respectively. The C_a–C_b distance increases from 1.33 to 1.43 Å, and then to 1.51 Å, respectively. These changes are parallel to the imaginary mode at TS, as shown in Table 1.

The energy barrier of this process calculated by the MP2 method (11.3 kcal mol^{-1}) is less than that calculated by the HF method (28.9 kcal mol^{-1}), which shows that the dynamical electron correlations are important for the TS, as generally recognized.

In the intermediate geometry shown in Fig. 2, one carbon atom C_a of ethylene is bound to the terminal oxygen atom O_b of the molecularly adsorbed oxygen. This state represents the intermediate not only for the epoxidation reaction, but also for acetaldehyde formation, as shown later. In this state, the π bond between C_a and C_b is formally broken, and the calculated energy barrier for the rotation around the C_a–C_b axis is small (calculated to be 2.3 kcal mol^{-1} by the HF method). This result agrees with the experimental finding that both *cis*- and *trans*-$C_2H_2D_2O$ molecules are produced from *cis*-$C_2H_2D_2$ in this catalytic reaction [7].

Table 1
Imaginary mode at the TS given in Fig. 2

TS structure	Eigenvalue	Term	Eigenvector
TS for approach	−0.127	C_a–O_b stretching	−0.946
		$H_aC_aC_bO_b$ torsion	0.215
		C_a–C_b stretching	0.168
TS for dissocation	−0.133	O_a–O_b stretching	0.879
		O_b–C_a–C_b bending	−0.211

When this intermediate is produced, the formation of ethylene oxide is an easy path, leaving the atomic oxygen on the Ag surface: the energy barrier of this process is only 3.1 kcal mol^{-1}. In this process, the O_a–O_b distance increases from 1.49 to 1.61 Å and then to infinity, and the O_b–C_b distance decreases from 2.44 to 2.37 Å and further to 1.47 Å. Note that the O–O distance of the free O_2^- is 1.35 Å. The mode of the negative force constant at TS shown in Table 1 certainly corresponds to this change of geometry (i.e. O_a–O_b stretching and O_b–C_a–C_b bending).

The reaction shown in Fig. 2 proceeds with $n=1$, i.e. with an excess electron supplied from the bulk metal, except for the free state. The heat of reaction is 37.1 kcal mol^{-1}, which represents the heat of reaction of gaseous ethylene oxide plus half of the dissociative adsorption energy of O_2 on Ag_2 (i.e. 21.5 and 15.6 kcal mol^{-1}, respectively, as obtained by the MP2 method).

Table 2 shows the net charge and the spin population of the $Ag_2O_2C_2H_4$ adcluster, calculated at the MP2 level, at several stages of the epoxidation reaction shown in Fig. 2. For the present system ($n=1$), the spin population is parallel with the frontier MO density, so that it reflects the reactivity. In the adsorbed superoxide state, the net charges of O_a and O_b are −0.558 and −0.217, respectively. On the other hand, the spin population of O_b (+0.784) is greater than that of O_a (+0.203), so that O_b should be more reactive than O_a. This result agrees with our previous theoretical result using a AgO_2 adcluster [42–44]: the reactivity is higher at the terminal oxygen than at the inner oxygen, while the charge is more negative on the inner oxygen.

The negative charges on the Ag atoms may be somewhat artificial, which is due to the use of a small Ag_2 cluster. We have previously investigated

Table 2
Net charge and spin population of the $Ag_2O_2C_2H_4$ adcluster, calculated at the MP2 level at the various structures shown in Fig. 3 for the epoxidation reaction of ethylene with molecularly adsorbed oxygen

	Adsorbed oxygen	TS for approach	Intermediate	TS for dissociation	Product
Net charge					
Ag_a	−0.028	−0.058	−0.054	−0.050	−0.058
Ag_b	−0.197	−0.270	−0.332	−0.345	−0.300
O_a	−0.558	−0.610	−0.609	−0.636	−0.642
O_b	−0.217	−0.311	−0.269	−0.241	−0.554
C_a	−0.356	−0.020	+0.035	+0.032	−0.109
C_b	−0.356	−0.450	−0.438	−0.440	−0.109
H_a	+0.178	+0.187	+0.160	+0.165	+0.193
H_b	+0.178	+0.187	+0.160	+0.165	+0.193
H_c	+0.178	+0.173	+0.173	+0.175	+0.193
H_d	+0.178	+0.173	+0.173	+0.175	+0.193
Spin population					
Ag_a	+0.182	−0.024	−0.015	+0.004	−0.108
Ag_b	−0.169	+0.040	+0.029	−0.001	+0.077
O_a	+0.203	+0.479	−0.048	+0.229	+1.031
O_b	+0.784	−0.192	+0.085	−0.192	0.0
C_a	0.0	−0.168	−0.113	−0.093	0.0
C_b	0.0	+0.992	+1.213	+1.205	0.0
H_a	0.0	+0.004	+0.006	+0.005	0.0
H_b	0.0	+0.004	+0.006	+0.005	0.0
H_c	0.0	−0.068	−0.082	−0.081	0.0
H_d	0.0	−0.068	−0.082	−0.081	0.0

O_2 adsorption on Ag_2 and Ag_4 clusters using the DAM [42–44]. Based on this experience, the energetics can safely be described by the present model as far as we adopt the DAM, although the net charges on Ag were better for the Ag_4 cluster than for the Ag_2 cluster [42–44]. On the other hand, the cluster model cannot give reasonable energetics, even if a moderately large cluster such as Ag_{24} [55] is used. Note that the net charges on the admolecules are not greatly affected by the cluster size in the DAM.

In the intermediate, on the other hand, the largest spin population of +1.213 is situated on C_b, particularly on the $2p_z$ orbital of C_b. From the adsorbed state to the intermediate, about one single spin moves from O_b to C_b: the reactive site shifts from O_b to C_b.

When the product (ethylene oxide) is formed from the intermediate, about one single spin moves from C_b to O_a, which is the atomic oxygen adsorbed on the surface. This spin mainly occupies the $2p_x$ orbital of O_a, while the $2p_y$ orbital is doubly occupied. This shows the reactivity of the atomically adsorbed oxygen, which is studied in Section 4.

For the occurrence of the epoxidation reaction, spin transfer seems to be important, as shown in Fig. 2 and Table 2. Positive spin exists on C_b and O_a and negative spin on C_a and O_b.

3.2. Acetaldehyde formation process

We now study the acetaldehyde formation process from ethylene and molecularly adsorbed superoxide on the Ag surface. When acetaldehyde is produced, it is readily oxidized to CO_2 and H_2O by combustion in the presence of oxygen: acetaldehyde is an intermediate in the complete oxidation process [56].

Fig. 3 shows the energy diagram for the formation of acetaldehyde calculated by the MP2 method. From the reactant to the intermediate, the pathway in Fig. 3 is the same as that in Fig. 2. In the next step, H_a bound to C_a in the intermediate

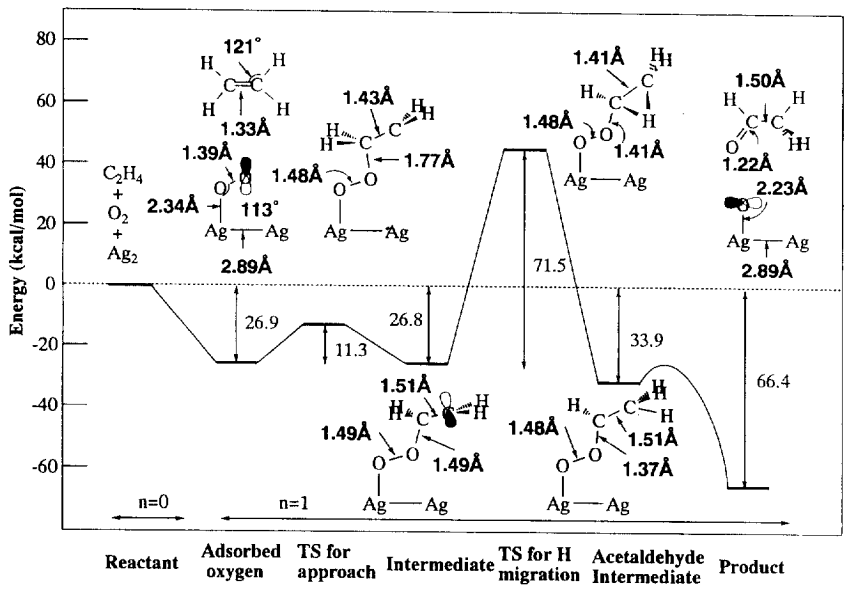

Fig. 3. Energy diagram for the acetaldehyde formation reaction from ethylene and molecularly adsorbed oxygen, calculated by the MP2 method.

migrates to C_b, which results in a stable conformation, denoted "acetaldehyde intermediate" in Fig. 3. When this acetaldehyde intermediate is formed, it is a rather easy pathway to give the complete oxidation products CO_2 and H_2O. However, the energy barrier for this H_a migration is very high (71.5 kcal mol^{-1}). This step is therefore forbidden energetically. This is another reason for the high selectivity of the epoxide formation process summarized in Section 3.1.

In the step from the intermediate to the acetaldehyde intermediate, the system has only C_1 symmetry and the C_a–C_b distance changes from 1.51 to 1.41 Å in the TS and then back to 1.51 Å in the acetaldehyde intermediate. The short bond length of 1.41 Å in the TS is due to the H_a bridging conformation, and the bond length of 1.51 Å is close to that in acetaldehyde (1.50 Å). On the other hand, the C_a–O_b bond length decreases from 1.49 to 1.41 Å in the TS and then to 1.37 Å in the acetaldehyde intermediate. It becomes 1.22 Å in the acetaldehyde molecule, in which C_a–O_b is a double bond.

Table 3 shows the net charge and the spin population calculated by the MP2 method. The net charge does not change significantly on each atom. However, the spin population and therefore the reactivity changes significantly: on C_a it changes from −0.113 to +0.994 in the TS, and then to +1.002 in the intermediate. On the C_b atom, it decreases from +1.213 to −0.126 and then to −0.113: about one spin moves from C_b to C_a as hydrogen migrates from C_a to C_b.

A large spin population on C_b in the intermediate reflects the high reactivity of the C_b atom. The reaction of the active C_b atom with O_b gives ethylene oxide, as shown in Fig. 2, and that with H_a gives acetaldehyde, as shown in Fig. 4. The energy barrier of the former reaction is 1.8 kcal mol^{-1}, and that of the latter is 71.5 kcal mol^{-1}. The difference between these barriers determines the selectivity of this reaction: the product of the reaction of ethylene with the molecularly adsorbed superoxide on a silver surface is ethylene oxide and not CO_2 and H_2O, the intermediate of which is acetaldehyde on the surface. This is one origin of the high selectivity of this reaction.

3.3. *Effect of the silver surface*

We investigate here the effect of the silver surface on the epoxidation reaction. The effect of the silver

Table 3
Net charge and spin population at some structures shown in Fig. 4 for the formation of acetaldehyde from ethylene and molecularly adsorbed oxygen

	Intermediate	TS for H migration	Acetaldehyde intermediate	Product
Net charge				
Ag_a	−0.054	−0.012	−0.027	−0.058
Ag_b	−0.332	−0.271	−0.285	−0.300
O_a	−0.609	−0.713	−0.690	−0.642
O_b	−0.269	−0.216	−0.196	−0.660
C_a	+0.035	+0.106	+0.154	+0.282
C_b	−0.438	−0.641	−0.695	−0.431
H_a	+0.160	+0.173	+0.156	+0.156
H_b	+0.160	+0.211	+0.228	+0.235
H_c	+0.173	+0.182	+0.182	+0.209
H_d	+0.173	+0.182	+0.172	+0.209
Spin population				
Ag_a	−0.015	−0.000	−0.020	−0.108
Ag_b	+0.029	−0.001	−0.018	+0.077
O_a	−0.048	+0.051	−0.056	+1.031
O_b	+0.085	+0.053	+0.054	0.0
C_a	−0.113	−0.994	+1.002	0.0
C_b	+1.213	−0.126	−0.113	0.0
H_a	+0.006	−0.086	−0.063	0.0
H_b	+0.006	−0.008	+0.005	0.0
H_c	−0.082	+0.061	+0.035	0.0
H_d	−0.082	+0.061	+0.027	0.0

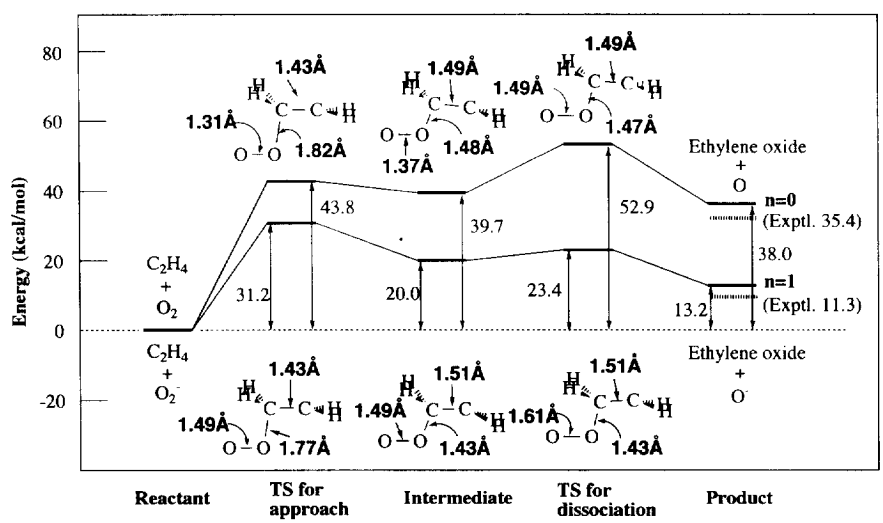

Fig. 4. Energy diagrams for the reactions between ethylene and gaseous oxygens (neutral O_2 ($n=0$) and O_2 anion ($n=1$)), calculated by the MP2 method. The upper geometries are for $n=0$, and the lower geometries are for $n=1$.

surface may be two-fold: (i) to provide the reaction site interacting with the surface atoms, and (ii) to provide electrons to the reaction site, as considered in the DAM.

Fig. 4 shows the energy diagram for the reaction between ethylene and gaseous oxygen without the silver surface, calculated by the MP2 method. Two energy diagrams correspond to the calculations with $n=1$ and $n=0$. The former involves an excess electron, but the latter is neutral. For $n=1$, we used the optimized geometries calculated for the $Ag_2O_2C_2H_4$ adcluster shown in Fig. 3. However, for $n=0$, the O–O distance of the free O_2 molecule (1.207 Å) is very different from the distance of the reaction intermediates and the TSs (1.39–1.61 Å) shown in Fig. 3. We therefore carried out geometry optimization for the intermediate and two TSs using the HF method. The schematic structures are illustrated in Fig. 4. The upper and lower geometries correspond to those for $n=0$ and $n=1$, respectively. For $n=0$, the O–O distance is calculated to be 1.37 Å for the intermediate, which is smaller than the corresponding value of 1.49 Å for $n=1$.

Comparing Fig. 4 with Fig. 2, we clearly see the catalytic activity of the silver surface for the epoxidation reaction. Without the surface, the reaction is endothermic and the pathway has large barriers. Electron transfer ($n=1$) certainly reduces the barrier, but the existence of and the direct interaction with the actual silver atoms on the surface are quite important. Clearly, the exothermicity of the reaction shown in Fig. 2 is due to the formation of atomically adsorbed oxygen on the surface. Thus, both of the effects summarized at the beginning of this subsection are the origin of the catalytic activity of the silver surface.

We now investigate Fig. 4 in more detail. The calculated energy barriers for $n=0$ are higher than those for $n=1$. The barriers for ethylene approach are 43.8 and 31.2 kcal mol^{-1}, respectively. From the intermediate to the product, the barrier for O–O bond dissociation is small, 3.4 kcal mol^{-1} for $n=1$, which is almost the same as that in Fig. 3 (3.1 kcal mol^{-1}). However, for $n=0$ the barrier is large (13.2 kcal mol^{-1}), and becomes the highest barrier in this pathway (52.9 kcal mol^{-1} higher than the reactant). The gaseous reaction is endothermic by 38.0 and 13.2 kcal mol^{-1} for $n=0$ and $n=1$, respectively, which are compared with experimental values of 35.4 and 11.3 kcal mol^{-1}, respectively.

4. Reactions with atomically adsorbed oxygen

The atomically adsorbed oxygen on the Ag surface is produced from the peroxide species of the molecularly adsorbed oxygen [42–44]. It is also produced, as shown in Fig. 2, as a product of the epoxidation reaction from ethylene and the molecularly adsorbed superoxide species. We study here the reactivity of the atomically adsorbed oxygen.

Fig. 5 shows the energy diagram for the reaction of ethylene with atomically adsorbed oxygen on the Ag surface calculated using the MP2 method. The geometries involved are optimized at the HF level, similar to the calculations for the molecularly adsorbed oxygen.

When ethylene oxide is generated out of the Ag surface after the surface reaction shown in Fig. 2, the atomically adsorbed oxygen O^- is left on the surface. For dissociative adsorption on the surface, the stabilization energy is calculated to be 31.2 kcal mol^{-1} (15.6 kcal mol^{-1} per O) by the MP2 method and 64.6 kcal mol^{-1} at the UHF level, the experimental value being 41–44 kcal mol^{-1} [34]. The dissociatively adsorbed species is more stable than the molecularly adsorbed species.

Table 4 shows the net charge and the spin population of each atom in the reaction between ethylene and atomically adsorbed oxygen. The net charge and the spin population of the atomically adsorbed oxygen O_a are -0.642 and $+1.031$, respectively. This spin population exists on the in-plane $2p_x$ orbital which is parallel to the Ag–Ag bond.

When ethylene attacks the atomic oxygen on the surface, the most favorable approach is to form the C_a–O_a bond, as illustrated in Fig. 5. It is similar to the approach of ethylene to the superoxide species shown in Fig. 2. The calculated energy barrier from the adsorbed oxygen to the intermediate is, however, as small as 1.5 kcal mol^{-1}, reflect-

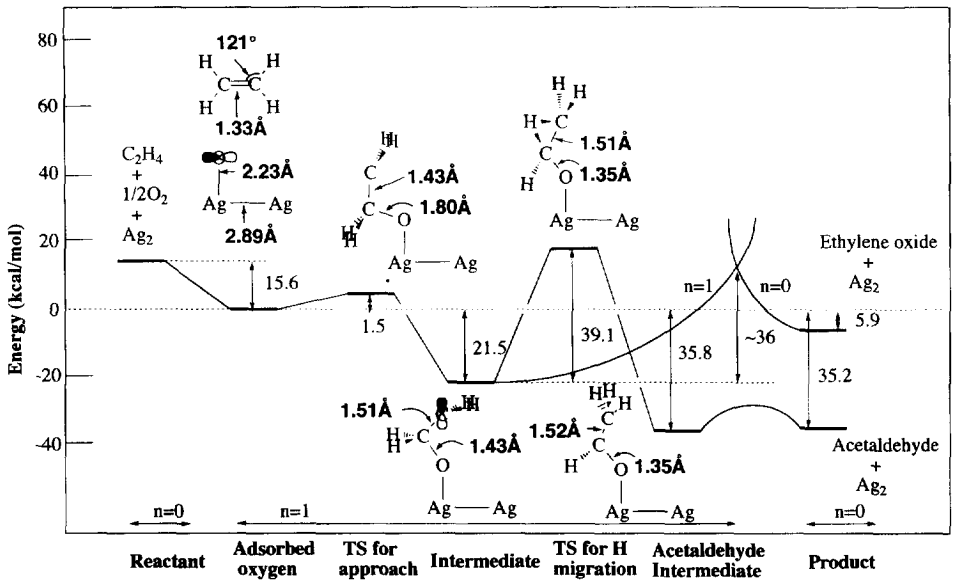

Fig. 5. Energy diagrams for the reaction between ethylene and atomically adsorbed oxygen, calculated by the MP2 method.

Table 4
Net charge and spin population of the $Ag_2OC_2H_4$ adcluster at various structures shown in Fig. 6 for the reaction of ethylene with dissociatively adsorbed oxygen

	Adsorbed oxygen	TS for approach	Intermediate	TS for H migration	Acetaldehyde intermediate
Net charge					
Ag_a	−0.058	−0.174	−0.197	−0.141	−0.172
Ag_b	−0.300	−0.251	−0.264	−0.252	−0.260
O_a	−0.642	−0.648	−0.654	−0.646	−0.621
C_a	−0.356	−0.105	+0.027	+0.039	+0.105
C_b	−0.356	−0.442	−0.432	−0.688	−0.677
H_a	+0.178	+0.147	+0.105	+0.135	+0.092
H_b	+0.178	+0.147	+0.105	+0.167	+0.151
H_c	+0.178	+0.163	+0.154	+0.168	+0.164
H_d	+0.178	+0.163	+0.154	+0.218	+0.218
Spin population					
Ag_a	−0.108	+0.015	+0.039	+0.000	−0.014
Ag_b	+0.077	+0.007	−0.014	+0.009	+0.013
O_a	+1.031	+0.344	+0.025	+0.111	+0.166
C_a	0.0	−0.207	−0.090	+0.422	+0.937
C_b	0.0	+0.957	+1.191	+0.553	−0.105
H_a	0.0	+0.005	+0.003	−0.007	−0.056
H_b	0.0	+0.005	+0.003	−0.046	+0.027
H_c	0.0	−0.063	−0.078	−0.010	+0.028
H_d	0.0	−0.063	−0.078	−0.032	+0.005

ing the reactivity of the atomic oxygen. The C_a–O_a bond is formed by the interaction between the p_x orbital of O_a and the π and π^* orbitals of ethylene. In the TS and the intermediate, the C_a–O_a distance is calculated to be 1.80 and 1.43 Å, respectively. The C–C bond changes from 1.33 Å in the TS to 1.51 Å in the intermediate: it changes from the double-bond length to the single-bond length. In the intermediate, the spin population of C_b is +1.191, which implies that the C_b atom is highly reactive. Up to this intermediate, the reaction proceeds quite smoothly.

The next step from this intermediate is very important, since it determines the selectivity of the reaction by the atomically adsorbed oxygen. If C_b attacks the oxygen to form the C_b–O_a bond, ethylene oxide is formed. If C_b attacks another C–H bond, causing hydrogen migration as in Fig. 3, acetaldehyde is a product, which is further transformed to CO_2 and H_2O, the complete oxidization product.

For the hydrogen migration reaction, the barrier is calculated to be 39.1 kcal mol^{-1}, which is high but lower than the barrier (71.5 kcal mol^{-1}) of the reaction in which the superoxide species is involved (see Fig. 3). The C–C distance does not change much in this process: it is 1.51 Å in the initial intermediate and in the TS for H migration, and 1.52 Å in the acetaldehyde intermediate. This process is calculated using an adcluster with $n=1$.

Unfortunately, the structure of the TS to form the C_b–O_a bond could not be determined by the geometry optimization procedure using both the $n=1$ and $n=0$ adclusters. If the pathway from the intermediate to the product (ethylene oxide) is one step, it is a quite interesting step since it involves both geometrical changes and one-electron back-transfer from the admolecule to the bulk metal. In the DAM picture, the intermediate in Fig. 5 is naturally described with $n=1$, i.e. with one additional electron supplied from the bulk to the adcluster, but the product (ethylene oxide plus Ag_2) should be neutral, i.e. $n=0$. If the TS lies in such a process, it might correspond to some partial number of n within the present DAM calculation. Otherwise, we have to use a sufficiently large cluster model which can represent the effect of the bulk metal. Here, we calculated two potential curves, one starting from the intermediate and the other from ethylene oxide plus Ag_2, using $n=1$ and $n=0$, respectively. All the geometrical parameters were assumed to change linearly, except for the Ag–O distance, which was kept at 2.180 Å.

The potential curve for $n=1$ increases monotonically from the intermediate to the product, while the curve for $n=0$ also increases monotonically from ethylene oxide and Ag_2 to the intermediate, and the two energy curves cross. The energy difference between the crossing point and the intermediate is $\sim$36 kcal mol^{-1}, which may be considered as the energy barrier of this process. At this "TS", one electron is transferred back to the metal.

The selectivity giving either ethylene oxide or acetaldehyde would be dependent on the heights of the barriers of the two processes and on the stabilities of the two products. The calculated energy barriers for the two processes are similar (39.1 and $\sim$36 kcal mol^{-1}, respectively). On the other hand, the energy differences between the two products and the intermediate are +15.6 and −13.7 kcal mol^{-1}, respectively, which means endothermicity and exothermicity from the intermediate, respectively. From the above data alone it is difficult to decide which is the preferential process, although acetaldehyde formation may be favorable for the exothermicity. However, it can safely be said that both ethylene oxide and acetaldehyde are formed from ethylene and atomically adsorbed oxygen on the Ag surface. This is in agreement with the observation by van Santen and de Groot [18] that both ethylene oxide and CO_2 were obtained from atomically adsorbed oxygen. Furthermore, this result is very important since it would be a reason for the experimental maximum selectivity of more than 6/7 [1–3]: the selectivity of superoxide is very high (say 99%) and the atomically adsorbed oxygen also contributes to this selectivity, even though its contribution is low, giving an overall selectivity of over 6/7.

Based on the above analysis, we further note that both electron acceptor and donor may work to reduce the barrier of the electron transfer step: they work to stabilize the $n=1$ and $n=0$ curves, respectively. The effects of Ce and halogens as promoters of catalysts are well known experimentally [1–3]. We speculate that these promoters act

in this electron-transfer step, giving ethylene oxide. The design of a promoter or co-catalyst which is effective in this electron-transfer step is of crucial importance, since it would be a key in increasing the selectivity to over 6/7.

Kilty et al. [16,17] assigned their IR peaks to the $Ag–O–CH_2–CH_2^-$ intermediate. This observation means that this intermediate has a lifetime which is long enough to be observed, which is in agreement with our result shown in Fig. 5: this intermediate is considerably stable (21.5 kcal mol^{-1}) and the barriers starting from this intermediate to acetaldehyde and to ethylene oxide are both rather high (39 and 36 kcal mol^{-1}, respectively).

5. Comparison with previous experimental and theoretical studies

Many experimental and theoretical researches have been performed to clarify the reaction mechanism of the silver-catalyzed epoxidation of ethylene. However, a mechanism totally consistent with all the observations seems not to have existed: there was even a conflict existed between the results. In this section, we try to explain many experimental results by comparing the present results with the previous experimental and theoretical findings.

An Eley–Rideal (ER) mechanism proposed by Twigg et al. [4], in which gas-phase ethylene reacts with the adsorbed oxygen, has been widely accepted because ethylene is not adsorbed on a clean silver surface [1–3,5,6]. The high temperature used in the experiments also supports the ER mechanism. However, a Langmuir–Hinshelwood (LH) mechanism was not ruled out, since ethylene adsorbs on an Ag^+ site induced by oxygen adsorption [5,6]. Therefore, we have checked the possibility of a reaction between the adsorbed oxygen and the adsorbed ethylene using an $Ag_2–O_2–C_2H_4$ adcluster with $n=0$ and $n=1$, but no stable geometries or species were found: the present calculation supports the ER mechanism.

Controversy still remains regarding the active oxygen species. Early studies concluded that the catalytic activity unique to silver is originated by the existence of molecularly adsorbed oxygen, which was not detected or rare on other metal surfaces. More direct evidence for molecular oxygen as the active species has been obtained by several experimental studies: for example, complete oxidation only occurs when a N_2O pulse giving atomically adsorbed oxygen is used, but the epoxidation reaction occurs when an O_2 pulse giving molecularly adsorbed oxygen is used, at least initially [9,10]. The assumption that molecular and atomic oxygen cause the partial and total oxidation reactions, respectively, has an upper limit for selectivity of 6/7. Recent experiments giving a selectivity higher than 6/7 may conflict with this assumption.

On the other hand, a mechanism assuming atomic oxygen as an active species was suggested from the experimental data that only atomically adsorbed oxygen exists at high temperature under industrial conditions, since molecular oxygen desorbs or dissociates. However, this mechanism may conflict with the surface dependence of the selectivity: the selectivity of partial oxidation is lower on Ag(110) than on Ag(111), although oxygen dissociation is preferred on Ag(110) [13]. Furthermore, a copper surface, which leads to the dissociative adsorption of O_2 more easily than silver, does not catalyze the epoxidation of ethylene. Formaldehyde formation from methanol, in which atomic oxygen is assumed to be an active species [57], is catalyzed not only by silver but also by copper.

In this paper, we have clarified theoretically that the selectivity of the molecularly adsorbed superoxide is high, and that of the atomically adsorbed oxygen is low. When an O_2 molecule is adsorbed on a Ag surface, the initial product will be the molecularly adsorbed end-on superoxide species, which is highly reactive with ethylene to give ethylene oxide. This reactivity and selectivity of the molecularly adsorbed superoxide explains the high selectivity of the silver catalyst. The result that atomically adsorbed oxygen can also give ethylene oxide, though in low selectivity, explains the experimental selectivity exceeding 6/7. Thus, the mechanism presented here can explain unambiguously the high selectivity of the silver catalyst.

Both superoxide and peroxide were observed on

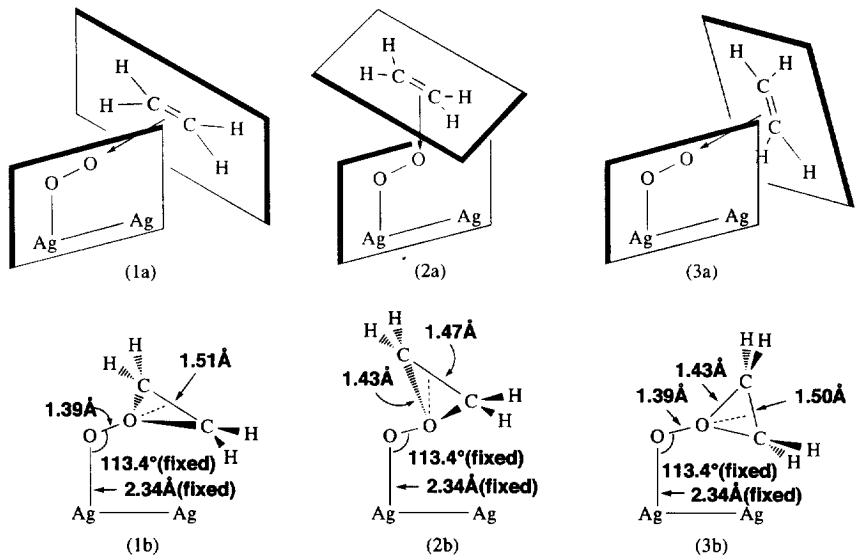

Fig. 6. Some other approaches of ethylene examined in this study. (1a) The C–C bond of ethylene is perpendicular to the C_s plane, and its π bond attacks terminal oxygen from the extension of the O–O bond. (2a) A similar attack to (1a), but from above the O–O bond. (3a) A similar attack to (1a) but the C–C bond of ethylene is coplanar with the C_s plane. (1b), (2b) and (3b) are the optimized geometries for these approaches.

a silver surface in many experiments [22–36]. The present study shows that the active species is the superoxide in the end-on structure, which has a spin on a terminal oxygen. This spin is transferred to ethylene in the ethylene-approaching process, giving Ag–O–O–CH_2–$CH_2^{\cdot}$ as an intermediate; a spin is transferred from the superoxide to the terminal carbon, which agrees with the IR experiment [16,17]. A low rotational barrier around the C–C single bond in this intermediate (calculated barrier of ~ 2 kcal mol^{-1}) should be a reason why *cis*-$C_2H_2D_2$ leads to both *cis*- and *trans*-$C_2H_2D_2O$ [7]. We have shown elsewhere that the ground state of the molecularly adsorbed oxygen is superoxide in the end-on structure and peroxide in the side-on structure [58], and that a barrier exists between them. Furthermore, the peroxide leads to dissociative adsorption [42–44], and the energy barrier for dissociation is calculated to be larger on the Ag(111) surface than on the Ag(110) surface [58], which explains the surface dependence of the selectivity in the epoxidation reaction.

The electronic structure of the active atomic species is the oxyradical anion, as clearly shown by Carter and Goddard [38,39]. They examined not only the on-top site but also the bridge and three-fold sites. They showed that hydrogen transfer from gaseous ethylene to oxyradical anion did not occur because of the instability of $C_2H_3^{\cdot}$ species. A spin transfer from the oxyradical anion to ethylene, giving the Ag–O–CH_2–$CH_2^{\cdot}$ intermediate, is important in both our studies and those of Carter and Goddard. Kilty et al. assigned their IR peaks to the Ag–O–CH_2–$CH_2^{\cdot}$ intermediate [16,17]. We obtain in Fig. 6 two comparable barriers for producing ethylene oxide and acetaldehyde from the intermediate. Since the process giving ethylene oxide involves the back-transfer of an electron from the adcluster to the bulk metal, we assumed the TS to be a crossover between the potential curves of $n=0$ and $n=1$. This barrier may therefore be sensitive to both electron donor and acceptor.

6. Conclusion

We summarize here our results on the mechanism of the partial oxidation reaction of ethylene on a silver surface. We performed calculations

Table 5
Comparison of the energy barrier and the heat of reaction for the epoxidation and acetaldehyde formation by molecularly and atomically adsorbed oxygen (kcal mol^{-1})

Reaction	Energy barrier	Heat of reaction[a]
Molecularly adsorbed oxygen		
$O_{2(a)}/Ag + C_2H_4 \rightarrow C_2H_4O + O_{(a)}/Ag$	11.3	10.2
$O_{2(a)}/Ag + C_2H_4 \rightarrow CH_3CHO + O_{(a)}/Ag$	71.5	39.5
Atomically adsorbed oxygen		
$O_{(a)}/Ag + C_2H_4 \rightarrow C_2H_4O + Ag$	≈ 36	21.5 (24.7)
$O_{(a)}/Ag + C_2H_4 \rightarrow CH_3CHO + Ag$	39.1	50.8 (52.3)
Without Ag surface (gas phase)		
$O_2^- + C_2H_4 \rightarrow O^- + C_2H_4O$	31.2	−13.2 (−11.3)
$O_2 + C_2H_4 \rightarrow O + C_2H_4O$	52.9	−38.0 (−35.4)

[a]Values in parentheses are experimental values.

using both the (U)HF and MP2 methods with the appropriate basis sets, and used the DAM to include the effect of the bulk metal. The present theoretical results support the mechanism summarized by Ayame [1–3].

The calculated energy barrier and the heat of reaction are summarized in Table 5. The primarily important species for the epoxidation of ethylene on a silver surface is the superoxide O_2^- which is molecularly adsorbed on the surface in the bent end-on geometry. Ethylene attacks the terminal oxygen atom of the superoxide, as shown in Fig. 2, with a barrier of about 11 kcal mol^{-1}, and then the reaction proceeds quite smoothly, leading to ethylene oxide. The overall reaction is exothermic by 37 kcal mol^{-1} from the $C_2H_4 + O_2 + Ag$ surface, or by 10 kcal mol^{-1} from C_2H_4 + superoxide on the Ag surface. The second exothermicity is due to the larger adsorption energy of the atomic oxygen as compared to the superoxide.

The complete oxidation of ethylene from the superoxide species on the Ag surface, which involves the acetaldehyde intermediate, is forbidden due to the existence of the large barrier (72 kcal mol^{-1}) in the hydrogen migration process, although this reaction is largely exothermic (by 66 kcal mol^{-1}) from the initial compounds, or by 40 kcal mol^{-1} from the superoxide on Ag and C_2H_4. This is one origin of the high selectivity observed experimentally.

When the silver surface is absent, the epoxidation reaction is very unfavorable, having a barrier of 53 kcal mol^{-1} and an endothermicity of 38 kcal mol^{-1} (see Fig. 4). The importance of the silver surface is quite evident. Among other factors, the existence of the superoxide species on the surface is very important for the catalytic activity of the silver surface.

The atomically adsorbed oxygen, which is left on the surface after completion of the epoxidation reaction by the superoxide, or which may exist by the dissociative adsorption of O_2 on the surface, has two reaction channels leading to ethylene oxide and to complete oxidation. The selectivity here seems to be small, and both products will be obtained. This could be the reason why some experiments reach a selectivity larger than 6/7. In the process leading to ethylene oxide, electron back-transfer from the reaction adsorbate complex to the metal surface should be important, and should be related to the barrier. Both electron donor and acceptor would be effective in reducing the barrier for this process.

Acknowledgements

We thank Professor A. Ayame and Dr. Z.M. Hu for valuable discussions. The calculations were performed using the computers at the Institute for Molecular Science. Part of this study was supported by a Grant-in-Aid for Scientific Research

from the Ministry of Education, Science, and Culture of Japan, and by the New Energy and Industrial Technology Development Organization (NEDO).

Appendix A: Accuracy of the present method

We show here the accuracy of the present basis functions and the effects of electron correlations. In the formation of ethylene oxide, the dissociation of the O–O bond may be considered as an important step. We calculated the dissociation energy (D_e) of O_2 and O_2^-, and the results are shown in Table 6 and Table 7, respectively, using the UHF, MP2, and MP4 methods with different basis functions:

BS1: [5s3p], Huzinaga–Dunning (9s5p)/[4s2p]+ diffuse s, p (0.059),
BS2: [5s3p1d], BS1 + polarization d (1.154),
BS3: [5s3p2d], BS1 + two polarization d (2.704, 0.535),
BS4: [5s3p3d], BS1 + three polarization d (3.660, 1.260, 0.440), and
BS5: [5s3p2d1f], BS3 + polarization f (1.350).

Both experimental and optimized O–O lengths were used in the calculations (for BS4 and BS5, experimental bond lengths only); the experimental lengths are 1.20741 Å for O_2 and 1.35 Å for O_2^- [59,60].

The UHF results for $D_e(O_2)$ and ($D_e(O_2^-)$) are much smaller than the experimental values, and even the sign of $D_e(O_2)$ is not reproduced with BS1. On the other hand, those calculated by the MP2 and MP4 methods are much closer to the experimental values. The differences between the MP2 and MP4 results are much smaller than those

Table 6
Dissociation energy of O_2 calculated with several basis functions using the UHF, MP2 and MP4 methods

Method	BS	E(O) (Hartree)	$E(O_2)$ (Hartree) (O–O bond length (Å)[a])	$D_e(O_2)$ (kcal mol^{-1})
UHF	BS1	−74.804012	−149.595524 (exp.[b])	−7.84
			−149.595528 (1.206)	−7.84
	BS2	−74.806822	−149.658475 (exp.[b])	+28.13
			−149.662293 (1.163)	+30.53
	BS3	−74.807736	−149.660738 (exp.[b])	+28.40
			−149.663514 (1.169)	+30.15
	BS4	−74.807760	−149.665337 (exp.[b])	+31.26
	BS5	−74.808921	−149.667989 (exp.[b])	+31.47
MP2	BS1	−74.851520	−149.828621 (exp.[b])	+78.80
			−149.845208 (1.344)	+89.21
	BS2	−74.908365	−150.003837 (exp.[b])	+117.41
			−150.005074 (1.235)	+118.18
	BS3	−74.918238	−150.026322 (exp.[b])	+119.13
			−150.027599 (1.249)	+119.93
	BS4	−74.924786	−150.045723 (exp.[b])	+123.09
	BS5	−74.946988	−150.094851 (exp.[b])	+126.05
MP4	BS1	−74.859509	−149.830090 (exp.[b])	+69.70
			−149.841669 (1.318)	+76.96
	BS2	−74.923683	−150.017556 (exp.[b])	+106.80
			−150.018213 (1.230)	+107.21
	BS3	−74.935289	−150.038251 (exp.[b])	+105.22
			−150.041771 (1.245)	+107.43
	BS4	−74.941697	−150.061982 (exp.[b])	+112.07
	BS5	−74.964227	−150.114240 (exp.[b])	+116.58
Exp.			(1.207)	+120.22

[a]Experimental or optimized O–O lengths.
[b]Experimental length is 1.20741 Å.

Table 7
Dissociation energy of O_2^- calculated with several basis functions using the UHF, MP2 and MP4 methods

Method	BS	$E(O^-)$ (Hartree)	$E(O_2^-)$ (Hartree) (O–O bond length (Å)[a])	$D_e(O_2^-)$ (kcal mol^{-1})
UHF	BS1	−74.784212	−149.597092 (exp.[b])	+5.56
			−149.597093 (1.349)	+5.57
	BS2	−74.786562	−149.630110 (exp.[b])	+23.05
			−149.633402 (1.292)	+25.11
	BS3	−74.787100	−149.631698 (exp.[b])	+23.13
			−149.634025 (1.301)	+24.59
	BS4	−74.787487	−149.633904 (exp.[b])	+24.26
	BS5	−74.788000	−149.636329 (exp.[b])	+24.73
MP2	BS1	−74.888183	−149.850143 (exp.[b])	+69.30
			−149.859620 (1.475)	+75.25
	BS2	−74.947918	−150.003564 (exp.[b])	+92.42
			−150.003885 (1.366)	+92.62
	BS3	−74.964441	−150.034193 (exp.[b])	+94.33
			−150.035120 (1.381)	+95.66
	BS4	−74.971494	−150.050921 (exp.[b])	+97.04
	BS5	−74.996000	−150.102911 (exp.[b])	+100.35
MP4	BS1	−74.898134	−149.857699 (exp.[b])	+62.79
			−149.866307 (1.499)	+68.19
	BS2	−74.962060	−150.020155 (exp.[b])	+73.93
			−150.020485 (1.373)	+84.55
	BS3	−74.979556	−150.052191 (exp.[b])	+86.19
			−150.053118 (1.388)	+86.77
	BS4	−74.987219	−150.070220 (exp.[b])	+88.67
	BS5	−75.011609	−150.124904 (exp.[b])	+93.54
Exp.			(1.35)	+96.06

[a]Experimental or optimized O–O length.
[b]Experimental length is 1.35 Å.

between the UHF and MP2 results, and the MP2 results are slightly larger than the MP4 results. Using BS1, the O–O bond lengths of O_2 and O_2^- are calculated to be about 0.1 Å longer than the experimental data by both the MP2 and MP4 methods. By adding d-functions, these values are improved and the discrepancies from the experimental values are less than 0.03 Å. These results show the importance of electron correlation and polarization functions for obtaining reasonable descriptions of the O–O bond. The present study uses the MP2 method and BS3, which gives $D_e(O_2)$ of 119.93 kcal mol^{-1} and $D_e(O_2^-)$ of 95.66 kcal mol^{-1}, in comparison with the experimental values of 120.22 [60] and 96.06 kcal mol^{-1}, respectively. The O–O bond lengths in the O_2 and O_2^- molecules are calculated to be 1.249 and 1.381 Å, respectively, in comparison with experimental values of 1.207 and 1.35 Å, respectively.

Table 8 shows the electron affinities of the oxygen atom ($EA(O)$) and the oxygen molecule ($EA(O_2)$) calculated by the UHF, MP2 and MP4 methods. Using the UHF method with BS1, $EA(O)$ is calculated to be −12.42 kcal mol^{-1}, which does not agree even in sign with the experimental value of 34.08 kcal mol^{-1} [61]. With the MP2 method, it is calculated to be 24.82 and 28.54 kcal mol^{-1} with BS2 and BS3, respectively. On the other hand, $^{EA}(O_2)$ is calculated to be 0.98 and −0.17 kcal mol^{-1} using the UHF method with BS1 and the MP2 method with BS2, respectively. The experimental value of $EA(O_2)$ is 9.92 kcal mol^{-1} [62], and it is only 4.94 kcal mol^{-1} using MP2 with BS3. Of these three calculations, only the MP2 method with BS3,

Table 8
Electron affinity of oxygen atom (EA(O)) and oxygen molecule ($EA(O_2)$)

Method	BS	EA(O) (kcal mol^{-1})	$EA(O_2)$ (kcal mol^{-1})
UHF	BS1	−12.42	+0.98
	BS2	−12.71	−17.80
	BS3	−12.95	−18.22
	BS4	−12.72	−19.72
	BS5	−13.13	−19.87
MP2	BS1	+23.01	+13.50
	BS2	+24.82	−0.17
	BS3	+28.54	+4.94
	BS4	+29.31	+3.26
	BS5	+30.76	+5.06
MP4	BS1	+24.24	+17.32
	BS2	+24.08	+1.63
	BS3	+27.78	+6.79
	BS4	+28.57	+5.17
	BS5	+29.73	+6.69
Exp.		+34.08	+9.92

which we adopted here, gives an acceptable result for the $EA(O_2)$ value.

We now examine the heat of reaction for the ethylene epoxidation reaction

$$CH_2=CH_2+\tfrac{1}{2}O_2\rightarrow C_2H_4O, \qquad (A.1)$$

the complete oxidation of ethylene,

$$CH_2=CH_2+3O_2\rightarrow 2CO_2+2H_2O, \qquad (A.2)$$

and acetaldehyde formation

$$CH_2=CH_2+\tfrac{1}{2}O_2\rightarrow CH_3CHO, \qquad (A.3)$$

by the HF, MP2 and MP4 methods. Table 9 shows the calculated heats of reactions for Eqs. (A.1)–(A.3) in comparison with the experimental data. The HF values are 3.05, 212.40 and 38.84 kcal mol^{-1}, respectively, which are much smaller than the experimental values of 24.67, 315.97 and 52.25 kcal mol^{-1}, respectively [1–3]. When one d function is added (BS2), the UHF values are not improved, but the MP2 values are improved. When two d functions are added (BS3), the MP2 results are in good agreement with the experimental values.

Considering the results shown in Tables 6–9, the MP2 calculations with BS3 give reasonable energetic results. However, for the optimized O–O bond lengths, the (U)HF results with BS1 agree better with experiments than the MP2 results with BS3. Therefore, we adopted the (U)HF method with BS1 for optimization and the MP2 method

Table 9
Heat of reaction for epoxidation and complete oxidation calculated by the HF, MP2 and MP4 methods with different basis functions for oxygen

Method	BS	Heat of reaction (kcal mol^{-1}) for		
		Epoxidation	Total oxidation	Acetaldehyde formation
HF	BS1	+3.05	+212.40	+38.84
	BS2	−0.07	+217.30	+36.85
	BS3	+5.50	+238.74	+37.74
	BS4	+4.68	+244.14	+40.33
	BS5	+6.41	+253.67	+40.80
MP2	BS1	+9.06	+261.57	+44.34
	BS2	+10.71	+276.72	+45.21
	BS3	+21.52	+312.24	+50.79
	BS4	+21.42	+320.12	+52.47
	BS5	+25.27	+339.38	+54.90
MP4	BS1	+15.85	+272.56	+51.28
	BS2	+15.40	+276.44	+50.33
	BS3	+30.51	+310.09	+60.33
	BS4	+30.67	+317.80	+62.35
	BS5	+35.69	+337.43	+65.86
Exp.		+24.67	+315.97	+52.25

with BS3 to calculate the energy values. Of course, the MP4 calculations with the larger basis sets such as BS4 or BS5 may give better results than the present choice. However, the improvements are rather small, verifying the present choice for minimizing computer time.

Appendix B: Other approaches of ethylene

Before performing the calculations reported in Fig. 2, we examined different approaches of ethylene to the molecularly adsorbed oxygen. The most favorable approach is shown in Fig. 2, and the other approaches are illustrated in Fig. 6. In approach (1a), the C=C axis is vertical to the C_s plane of Ag_2O_2 and ethylene approaches along the extension of the O–O axis. In approach (2a), the C=C axis is vertical to the C_s plane and ethylene approaches from above the adsorbed oxygen. In approach (3a), the C=C axis is in-plane and ethylene approaches along the extension of the O–O axis. The optimized geometries for all three approaches were calculated by the HF method using the basis set BS1, explained in Appendix A, and the resultant geometries are shown in (1b), (2b), and (3b) of Fig. 6.

For approach (1a), the energy of the optimized geometry is 91.1 kcal mol^{-1} higher than that of the adsorbed oxygen shown in Fig. 3. This high energy is easily understood from the MO interactions. The out-of-plane π^* orbital of O_2 interacts with the in-plane π^* orbital (LUMO) of ethylene. The in-plane π orbital (HOMO) of ethylene can interact only with the $2p\sigma^*$ orbital of O_2, whose energy is much higher. This causes electron transfer only from oxygen to ethylene, so that this approach is very unfavorable.

The optimized geometry (approach (2b)) for approach (2a) is 75.1 kcal mol^{-1} higher than that of the adsorbed oxygen. For approach (3a), the energy of the optimized structure is 103.9 kcal mol^{-1} higher than that of the adsorbed oxygen. In this approach, the HOMO of ethylene can interact only with the $2p\sigma^*$ orbital of O_2, which is very unfavorable, as in approach (1a). Thus, we conclude that only the approach shown in Fig. 2 is acceptable.

References

[1] A. Ayame, in: Y. Murakami (Ed.), Series of Lectures on Catalysis VII, Fundamental Industrial Catalytic Reaction, Catalytic Society of Japan, Tokyo, 1985, pp. 170–185 (in Japanese).
[2] A. Ayame, H. Kanoh, Shokubai 20 (1978) 381.
[3] H. Miura, A. Ayame, H. Kanoh, K. Miyahara, I. Toyoshima, Shinku 25 (1982) 302.
[4] G.H. Twigg, Proc. R. Soc. London Ser. A 188 (1946) 92.
[5] E.L. Force, A.T. Bell, J. Catal. 38 (1975) 440.
[6] E.L. Force, A.T. Bell, J. Catal. 40 (1975) 356.
[7] N.W. Cant, W.K. Hall, J. Catal. 52 (1978) 81.
[8] W. Herzog, Ber. Bunsenges. Phys. Chem. 74 (1970) 216.
[9] M. Kobayashi, M. Yamamoto, H. Kobayashi, in: Proceedings of the Sixth International Congress on Catalysis, 1976, p. A24.
[10] M. Kobayashi, in: A.T. Bell, L.L. Hegedus (Eds.), Catalysis Under Transient Conditions, American Chemical Society, Washington, DC, 1982, p. 209.
[11] S. Tanaka, T. Yamashita, J. Catal. 33 (1974) 392.
[12] S. Yokoyama, K. Miyahara, J. Res. Inst. Catal. Hokkaido Univ. 22 (1974) 63.
[13] C.T. Campbell, J. Catal. 94 (1985) 436.
[14] A. Ayame, N. Takeno, H. Kanoh, J. Chem. Soc., Chem. Commun. (1982) 617.
[15] A. Ayame, T. Kimura, M. Yamaguchi, H. Miura, N. Takeno, H. Kanoh, I. Toyoshima, J. Catal. 79 (1983) 233.
[16] P.A. Kilty, W.M.H. Sachtler, Catalysis Reviews, vol. 10, Marcel Dekker, New York, 1970, p. 1.
[17] P.A. Kilty, N.C. Rol, W.M.H. Sachtler, in: Proceedings of the Fifth International Congress on Catalysis, 1972.
[18] R.A. van Santen, C.P.M. de Groot, J. Catal. 98 (1986) 530.
[19] J. Yang, J. Deng, X. Yuan, S. Zhang, Appl. Catal. A 92 (1992) 73.
[20] J. Deng, J. Yang, S. Zhang, X. Yuan, J. Catal. 138 (1992) 395.
[21] Y. Peng, S. Zhang, L. Tang, J. Deng, Catal. Lett. 12 (1992) 307.
[22] D. Schmeisser, J.E. Demuth, Ph. Avouris, Phys. Rev. B 26 (1982) 4857.
[23] C. Pettenkofer, I. Pockrand, A. Otto, Surf. Sci. 135 (1983) 52.
[24] C. Pettenkofer, J. Eickmans, U. Erturk, A. Otto, Surf. Sci. 151 (1985) 9.
[25] A. Sexton, R.J. Madix, Chem. Phys. Lett. 76 (1980) 294.
[26] C. Backx, C.P.M. de Groot, P. Biloen, Surf. Sci. 104 (1981) 300.

[27] C. Backx, C.P.M. de Groot, P. Biloen, Appl. Surf. Sci. 6 (1980) 256.
[28] D.A. Outka, J. Stöhr, W. Jark, P. Stevens, J. Solomon, R.J. Madix, Phys. Rev. B 35 (1987) 4119.
[29] J. Stöhr, D.A. Outka, Phys. Rev. B 36 (1987) 891.
[30] H.A. Engehardt, A.M. Bradshaw, D. Menzel, Surf. Sci. 40 (1973) 410.
[31] P.B. Clarkson, A.C. Cirillo Jr., J. Catal. 33 (1974) 392.
[32] M.A. Barteau, R.J. Madix, Chem. Phys. Lett. 97 (1983) 85.
[33] K.C. Prince, A.M. Bradshaw, Surf. Sci. 126 (1983) 49.
[34] C.T. Campbell, Surf. Sci. 157 (1985) 43.
[35] K. Bange, T.E. Madey, J.K. Sass, Chem. Phys. Lett. 113 (1985) 56.
[36] A. Pushmann, J. Haase, Surf. Sci. 144 (1984) 559.
[37] M.A. Barteau, R.J. Madix, in: D.A. King, D.P. Woodruff (Eds.), The Chemical Physics of Solid Surfaces and Heterogeneous Catalysis, vol. 4, Elsevier, Amsterdam, 1982.
[38] E.A. Carter, W.A. Goddard III, Surf. Sci. 209 (1989) 243.
[39] E.A. Carter, W.A. Goddard III, J. Catal. 112 (1988) 80.
[40] P.J. van den Hoek, E.J. Baerends, R.A. van Santen, J. Phys. Chem. 93 (1989) 6469.
[41] K.A. Jørgensen, R. Hoffmann, J. Phys. Chem. 94 (1990) 3046.
[42] H. Nakatsuji, H. Nakai, Can. J. Chem. 70 (1992) 404.
[43] H. Nakatsuji, H. Nakai, Chem. Phys. Lett. 174 (1990) 283.
[44] H. Nakatsuji, H. Nakai, J. Chem. Phys. 98 (1993) 2423.
[45] H. Nakatsuji, J. Chem. Phys. 87 (1987) 4995; H. Nakatsuji, H. Nakai, Y. Fukunishi, J. Chem. Phys. 95 (1991) 640.
[46] H. Nakatsuji, Prog. Surf. Sci. 54 (1997) 1.
[47] H. Nakatsuji, R. Kuwano, H. Morita, H. Nakai, J. Mol. Catal. 82 (1993) 211.
[48] M.J. Frisch, M.H. Gordon, G.W. Trucks, J.B. Foresman, H.B. Schlegel, K. Raghavachari, M.A. Robb, J.S. Binkley, C. Gonzalez, D.J. Defrees, D.J. Fox, R.A. Whiteside, R. Seeger, C.F. Melius, J. Baker, R.L. Martin, J.J.P. Stewart, S. Topol, J. Pople, GAUSSIAN92, Gaussian Inc., Pittsburgh, PA, 1992.
[49] P.J. Hay, W.R. Wadt, J. Chem. Phys. 82 (1985) 270.
[50] S. Huzinaga, J. Chem. Phys. 42 (1965) 1293.
[51] T.H. Dunning Jr., J. Chem. Phys. 53 (1970) 2823.
[52] T.H. Dunning, Jr., P.J. Hay, in: H.F. Scaeffer III (Ed.), Modern Theoretical Chemistry, vol. 3, Plenum, New York, 1977, p. 10.
[53] S. Huzinaga, Gaussian Basis Sets for Molecular Calculations, Physical Science Data, vol. 16, Elsevier Science, Amsterdam, p. 23.
[54] X. Bao, J. Deng, S. Dong, Surf. Sci. 163 (1985) 444.
[55] T.H. Upton, P. Stevens, R.J. Madix, J. Chem. Phys. 87 (1987) 3143.
[56] L.Ya. Margolis, Adv. Catal. 14 (1963) 429.
[57] H. Nakai, S. Kaimori, A. Matsubara, H. Nakatsuji, to be submitted.
[58] H. Nakatsuji, Z.M. Hu, H. Nakai, K. Ikeda, K., Surf. Sci., in press.
[59] G. Herzberg, Spectra of Diatomic Molecules, Van Nostrand, Princeton, NJ, 1950.
[60] K.P. Huber, G. Herzberg, Constants of Diatomic Molecules, Van Nostrand Reinhold, New York, 1979.
[61] R.S. Berry, J.C. Mackie, R.L. Taylor, R. Lynch, J. Chem. Phys. 43 (1965) 3067.
[62] P.H. Krupenie, J. Phys. Chem. Ref. Data 1 (2) (1972) 423.